Fundamental studies in nanosciences at the Institute of Electronics, Microelectronics, and Nanotechnology (IEMN)

G. Allan, S. Barbet, Y. Coffinier, C. Delerue*, D. Deresmes, M. Diarra, H. Diesinger, B. Grandidier, L. Marcon and T. Mélin

IEMN – Départment ISEN – UMR CNRS 8520,
41 boulevard Vanban – 59046 Lille Cedex, France
Fax: +33 3 20 30 40 51
E-mail: guy.allan@isen.iemn.univ-lille1.fr
E-mail: sophie.barbet@isen.iemn.univ-lille1.fr
E-mail: yannick.coffinier@isen.iemn.univ-lille1.fr
E-mail: christophe.delerue@isen.fr
E-mail: dominique.deresmes@isen.iemn.univ-lille1.fr
E-mail: mamadou.diarra@isen.fr
E-mail: heinrich.diesinger@isen.iemn.univ-lille1.fr
E-mail: bruno.grandidier@isen.iemn.univ-lille1.fr
E-mail: lionel_bl@yahoo.fr
E-mail: thierry.melin@isen.iemn.univ-lille1.fr
Website: http://www.isen.fr/~delerue
*Corresponding author

O. Melnyk

Institut de Biologie de Lille,
UMR CNRS 8161, 1 rue du Professeur Calmette,
59021 Lille Cedex, France
E-mail: oleg.melnyk@ibl.fr
Website: http://www.gfpp.free.fr

D. Stiévenard, L. Wirtz and M. Zdrojek

IEMN – Départment ISEN – UMR CNRS 8520,
41 boulevard Vanban – 59046 Lille Cedex, France
E-mail: didier.stievenard@isen.iemn.univ-lille1.fr
E-mail: ludger.wirtz@isen.iemn.univ-lille1.fr
E-mail: zdrojek@if.pw.edu.pl

Abstract: This paper gives an overview over the fundamental research in nanosciences at the Institute of Electronics, Microelectronics and Nanotechnology (IEMN). We present some highlights from the numerical simulation of the electronic structure of nanowires and nanotubes, the charge

spectroscopy of Si nanoparticles and C nanotubes, the scanning tunnelling spectroscopy of semiconductor quantum dots, to research in surface science for bio-screening.

Keywords: nanowire; nanotube; bio-sensor; nanocrystal; simulation; STM; AFM; nano-electrodes.

Reference to this paper should be made as follows: Allan, G., Barbet, S., Coffinier, Y., Delerue, C., Deresmes, D., Diarra, M., Diesinger, H., Grandidier, B., Marcon, L., Mélin, T., Melnyk, O., Stiévenard, D., Wirtz, L. and Zdrojek, M. (2008) 'Fundamental studies in nanosciences at the Institute of Electronics, Microelectronics, and Nanotechnology (IEMN)', *Int. J. Nanotechnol*., Vol. 5, Nos. 6/7/8, pp.631–648.

Biographical notes: Guy Allan is Research Director at CNRS studying the Electronic Structure of Semiconductor Nanostructures. He received his PhD in Physics from the University of Paris-Sud, Orsay, France in 1970 for his research on the electronic structure of transition metals surfaces. He has authored over 250 technical publications.

Sophie Barbet is preparing her PhD at IEMN on the Development of KFM and EFM methods and their applications to the study of fundamental physical properties of semiconductor nanoparticles and the characterisation of GaN based devices.

Yannick Coffinier is a postdoctoral fellow at IEMN, where he is developing biosensors on semiconducting surfaces for medical application such as serodiagnosis. He received a PhD in Biochemistry from the University of Technology of Compiegne, France.

Christophe Delerue is a Scientist at the Institute of Electronics, Microelectronics, and Nanotechnology (IEMN, Lille), Director of Research at CNRS, and Professor at the Institut d'Electronique et du Numérique (ISEN, Lille). He obtained his PhD Degree in Materials Science at the University of Lille in 1989. His current research involves the theoretical simulation of nanoscale structures like semiconductor nanocrystals and nanowires. He has contributed over 110 publications to this field.

Dominique Deresmes is a Staff Scientist in the Physics Department at the Institute of Electronics, Microelectronics and Nanotechnology (IEMN). He received his Master Degree in Electronics from the University of Lille in 1990. He is currently responsible for the development and maintenance of the scanning probe microscopes in the institute.

Mamadou Diarra studied Science at the Universities of Bamako and Paris-Sud (Orsay), and received a MSc in Materials Science at the University of Paris-Sud. He is presently preparing a PhD concerning the theoretical simulation of the electronic structure and transport properties of semiconductor nanowires.

Heinrich Diesinger is CNRS Research Scientist at IEMN. He received his PhD in Microelectronics from the University Joseph Fourier Grenoble in 2001 for the development of NSOM at the semiconductor-electrolyte interface. His topics of interest are the development of EFM and KFM instrumentation and its application to semiconductor nanowires and nanotubes, and their handling by dielectrophoresis and Langmuir Blodgett techniques to organise them at large scale.

Bruno Grandidier is a Research Scientist in the Physics Department at the Institute of Electronics, Microelectronics and Nanotechnology (IEMN). He earned his PhD in Materials Science from the University of Lille in 1997. His current research program focuses on the growth and electrical characterisation of inorganic nanostructures.

Lionel Marcon received a PhD in Physical Biochemistry from the University of Lille, France in 2006 for his research on the electrical detection of biomolecules using silicon biosensors. He's currently working as a postdoctoral fellow at the University of Queensland, Brisbane, Australia on the application of barcoded silica particles for viral protease mapping.

Thierry Melin is CNRS permanent Research Scientist at IEMN working on the electronic and electrostatic properties of nanostructures and on scanning force microscopy techniques. He obtained his PhD Degree from the Ecole Polytechnique, Palaiseau, France on the optical properties of excitonic systems and electron gases in self-assembled low-dimensionality semiconductor structures.

Oleg Melnyk is Director of Research at CNRS. He is member of the scientific board of Bioconjugate Chemistry (*Journal of the American Chemical Society*) since 2004 and member of the scientific board of Groupement Français des Peptides et Protéines. His current research program is the development of novel peptide site-specific ligation chemistries and the design of microarray technologies. He has authored 73 publications and holds 11 patents.

Didier Stiévenard is a Senior Scientist in the field of Experimental Physics of Nanostructures, Director of Research at CNRS and in the research staff of Institut d'Electronique et du Numérique (ISEN). He received his PhD in Physics of Semiconductors in 1982. His current research is in the electronic structure of nanostructures (mainly nanoparticles, quantum dots, nanowires) using STM technique and on the electrical detection of biomolecular interaction assisted by NP. He has authored over 165 publications.

Ludger Wirtz studied Physics at Bonn University, Germany, and at the University of Tennessee in Knoxville, USA. He received the PhD from the Vienna University of Technology, Austria, in 2001. After a postdoctoral stay at the University of the Basque Country, San Sebastian, Spain, he joined the IEMN as a CNRS researcher in 2004. His research interests include semiclassical methods in mesoscopic physics, the theory of ion-surface interaction, and the theory of spectroscopy of nanostructures.

Mariusz Zdrojek obtained an International PhD Degree from Warsaw University of Technology and from The University of Lille for his work on the electrostatic and optical properties of carbon nanotubes probed by Electrostatic Force Microscopy and Raman spectroscopy. He has been appointed since 2007 as Assistant Professor at Warsaw University of Technology.

1 Introduction

The Institute of Electronics, Microelectronics and Nanotechology (IEMN) has been engaged for more than ten years in advanced research in nanoscience and nanotechnology. These activities take advantage of the proximity between physicists,

chemists and researchers in microelectronics, between theoreticians and experimentalists, allowing to combine long-term fundamental studies and more applied research. On the more fundamental side, IEMN's activities are engaged along several directions:

- growth and physics of heterostructures and nanostructures of semiconductors
- optical spectroscopy, scanning tunnelling microscopy (STM) and spectroscopy, detection and spectroscopy of charges in nanostructures
- physics of surfaces for bio-screening
- molecular electronics
- growth, characterisation and simulation of high-k dielectrics and ferroelectrics
- physics of waves in micro- and nano-structured materials.

The objective of this article is to present a selection of recent works which illustrates these activities and which has been undertaken by the researchers of the Physics Group of the institute. This selection includes four contributions:

- the theory and the numerical simulation of one-dimensional (1D) nanostructures
- the charge spectroscopy of nanostructures
- the STM spectroscopy of semiconductor nanocrystals
- recent activities at the interface between physics and biology, in collaboration with partner laboratories.

2 Theory and numerical simulation of one-dimensional (1D) nanostructures

One-dimensional nano-objects like nanotubes (C, BN) and semiconductor nanowires [1] receive increasing attention due to their potential applications in electronics, opto-electronics and sensors. We review in this section recent theoretical works we have performed in this field, illustrating the capabilities of *ab-initio* and semi-empirical methods to simulate the electronic and optical properties of nano-objects. Two systems will be considered in the following, Si nanowires and BN nanotubes.

One interest in semiconductor nanowires (SNWs) is the possibility to control their electrical properties by doping [2,3]. But, from experiments, it is not clear how the electrical conductivity of SNWs depends on the doping level. Most of the works showing good transport properties concern highly doped SNWs, above the metal-nonmetal transition. Otherwise, there are indications that the conductivity of the SNWs is extremely low [3]. Therefore the problem of the doping efficiency in SNWs has to be carefully considered.

In bulk semiconductors, the physics of shallow impurities is described in textbooks. The impurity gives rise to bound states in the energy gap but the impurity potential is strongly screened (dielectric constant $\varepsilon \sim 10$–20) and the ionisation energy is only of a few hundredths of an electron-volt so that the impurity is ionised at room temperature. We will see that the situation is different in a wide range of wire sizes because the ionisation energy of the impurities is greatly enhanced.

We calculate the electronic states of donors and acceptors in Si nanowires (SiNWs) using a tight binding (TB) method. TB allows the study of shallow impurities in bulk semiconductors [4] and is very well adapted to semiconductor nanostructures. The TB Hamiltonian is written as $H = H_0 + U_{imp} + \Sigma$ where H_0 is the Hamiltonian of the perfect wire [5]. U_{imp} is the potential induced by the impurity. It is obtained as the solution of the Poisson equation in which the system is represented by a cylinder of radius R and of dielectric constant ε_{in} embedded in a medium of dielectric constant ε_{out}. We use the bulk experimental value $\varepsilon_{in} = 11.7$ which is fully justified when $R > 2$ nm [5]. The last term Σ in the TB Hamiltonian is the self-energy potential which represents the interaction between the carrier and the surface polarisation charges induced by its own presence [5].

We present in Figure 1 the ionisation energy E_I of donor impurities located at the centre of free-standing SiNWs ($\varepsilon_{out} = 1$). High values of E_I are predicted, even for large SiNWs ($R > 5$ nm) in which the effect of quantum confinement is weak (see the shift of the conduction band edge due to quantum confinement, dashed line in Figure 1). Similar results are obtained for different positions of the impurities and also for acceptors [6]. E_I is enhanced due to the so-called dielectric confinement which appears when there is an important dielectric mismatch between the wire and its surroundings. At the impurity site, the nucleus charge ($+e$) is strongly screened ($=e/\varepsilon_{in}$), but the remaining charge [$+e(1 - 1/\varepsilon_{in})$] is repelled at the nanowire surface close to the impurity while it is at infinity in the bulk case. Thus the Coulomb interaction is strongly enhanced in a nanowire compared to the bulk. Figure 1 shows that the doping efficiency at 300 K of a P impurity at the centre of a SiNW is below 50% for $R < 9$ nm and below 0.1% for $R < 2$ nm when the nanowire is in vacuum. We also obtain that E_I strongly depends on dielectric constant of the surrounding materials, becoming smaller at increasing ε_{out}. We conclude that the transport properties of SNWs strongly differ from those of the bulk materials because donor and acceptor impurities may be electrically inactive. The transport properties also depend on the dielectric environment of the SNWs [6].

Figure 1 Ionisation energy E_I vs. the wire radius R for donor impurities (P = +, As = ×, Sb = ŏ) located along the axis of a free-standing SiNW. The bulk values are equal to 45 meV for P, 54 meV for As and 39 meV for Sb. Dashed line: shift of the conduction band edge due to quantum confinement. Doping efficiency (diamond): probability of ionisation towards the conduction band for a P impurity (300 K)

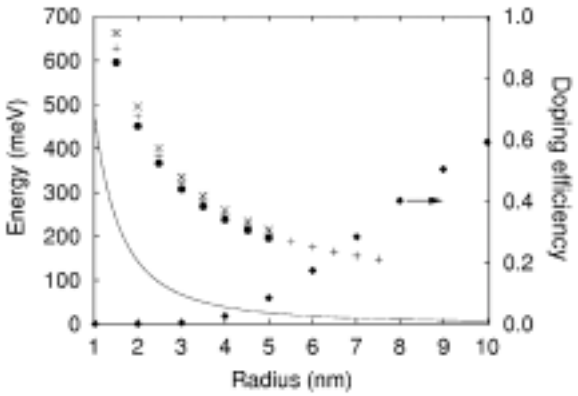

As an example for the calculation of optical properties of 1-dimensional nanostructures, we present our recent work on boron nitride (BN) nanotubes. BN nanotubes are isoelectronic to carbon nanotubes but have a uniform large band-gap (>6 eV). First predicted in 1994 [7] and produced in 1995 [8], BN nanotubes are now commonly produced in gram quantities [9]. In France, an important production site is the LEM, Onera, Châtillon. Like carbon nanotubes, BN tubes are frequently characterised by optical spectroscopy such as Raman spectroscopy and optical absorption. For the interpretation of the spectra, we have performed *ab initio* calculations (using density-functional theory) which yield the energies of vibronic excitations (phonons) and electronic excitations (excitons) as a function of the nanotube diameter and its chirality.

The phonon calculations [10] enabled us to compare with the experimental Raman spectra obtained at LEM. The position of the dominant high-frequency peak in the spectra depends sensitively on the curvature of the tubes and allows to unambiguously distinguish between the spectra of tubes and of hexagonal BN-particles in the BN nanotube samples [11].

The interpretation of optical absorption spectra of BN nanotubes [12] is considerably more involved (see Figure 2). In the simplest approximation (the so called Random-Phase approximation, RPA), a photon is absorbed by an electron transition from the valence to the conduction band with energy $\omega_{cv} = h\nu$.

Figure 2 Sketch of the different levels of approximation for electronic excitations: (a) independent electron transitions (random-phase approximation); (b) enlargement of the band-gap due to electron-electron correlation and (c) formation of a bound exciton by electron-hole interaction

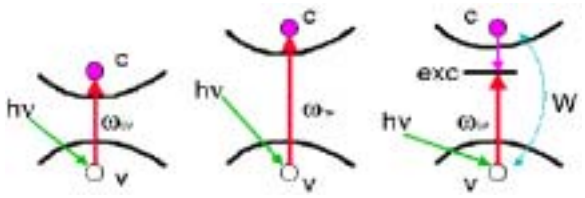

In many materials, however, this simple picture breaks down due to two effects:

- The band gap is usually not well described by density-functional theory [13] (which is a valid approximation only for the ground-state). Self-energy effects (electron-electron correlation) lead to an enlargement of the band-gap. This effect is particularly pronounced in low-dimensional nanostructures [14] where the excited electron interacts with its self-image charge on the surface of the structure.
- The excited electron interacts with the hole in the valence band through a screened Coulomb potential W. This can lead to bound excitonic states in the band-gap.

Using the techniques of many-body perturbation theory for the inclusion of electron-electron correlation [13] and of electron-hole interaction [13], we have shown that the spectra of bulk hBN and of the tubes are dominated by strong excitonic effects (see Figure 3). Furthermore, comparing the spectra of bulk hBN, of a single-sheet of hBN and of BN tubes, we have demonstrated the effect of the dimensionality: with reduced dimensionality, the binding energy of the excitons increases considerably (from 0.7 eV in bulk BN, via 2 eV in the 2-dim. single sheet to more than 3 eV for the

1-dim. tubes) [15]. At the same time, however, electron-electron correlation increases the quasi-particle band-gap [13] (calculated through the GW-method). The two effects (increased exciton-binding energy and increased band-gap) almost cancel each other. The dominant absorption peak remains therefore constant in position. The resulting optical gap (i.e., the onset of absorption) therefore remains constant as well as was indeed observed in recent EELS experiments [16].

Figure 3 Comparison of the spectra of: (a) bulk hBN; (b) a single sheet of hBN and (c) different BN-nanotubes. In the left panel, we show the spectra calculated in the random-phase approximation. In the right panel, we have included the effects of electron-electron and electron-hole correlation. Solid lines: spectra calculated with a broadening of 0.01 eV, dashed lines: broadening of 0.1 eV (for colours see online version)

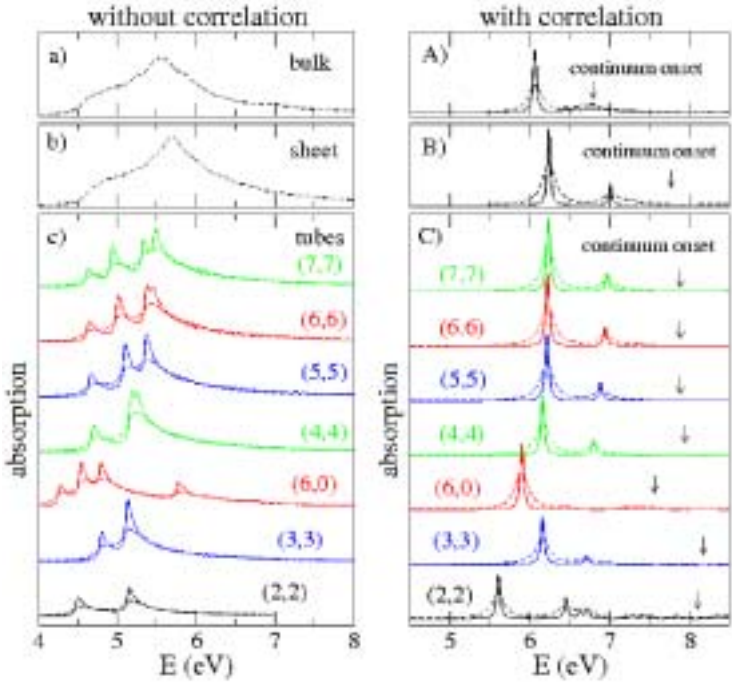

3 Electrostatic force microscopy of nanostructures

We have developed experiments aiming to probe the local electronic properties of nanostructures on insulators. Such experiments are based on the use of an atomic force microscope (AFM) operated in one of its electrical modes: Electrostatic Force Microscopy (EFM), Kelvin Force Microscopy (KFM), etc … In this section, we review results based on charge injection and EFM experiments applied to 0D and 1D nanostructures such as silicon nanoparticles and carbon nanotubes.

Experimentally, the tip of the EFM cantilever is used to address a single nanostructure, and inject charges when pressed with a few nN force and biased with respect to the substrate at an injection voltage V_{inj} [17]. In this process, charges are transferred (in most cases from the EFM tip into the nanostructure). We then use the set-up in the EFM mode as described in Figure 4, in order to detect the presence of

charges. EFM data consist in the shift of the resonance frequency f_0 of the cantilever, when biased at a detection voltage V_{EFM}. EFM frequency shifts are proportional to the gradient of the electrostatic force acting on the EFM tip, and can be split into three components:

- a capacitive contribution proportional to V_{EFM}^2, which comes from the attraction between capacitive charges on the tip and on the substrate
- an image charge contribution between the stored charge Q and its EFM tip image : this force gradient is proportional to Q^2, and does not depend on the EFM tip bias V_{EFM}
- a cross-term proportional to $V_{EFM} \times Q$, corresponding to the interaction between the stored charge Q, and capacitive charges at the tip apex.

These interactions have been dissociated experimentally [18] in the case of single nanoparticles separated from a conductive substrate (in practice, *p*-doped silicon) by a ultra thin (1–2 nm) tunnel oxide. In this configuration, the stored charge Q is screened by conductive substrate, and rather appears in electrostatic experiments as a surface dipole, of magnitude $Q \times h/\varepsilon$, where h is the nanoparticle height, and ε its dielectric constant. Therefore, the three electrostatic force contributions described above correspond to

- charge-charge interactions proportional to V_{EFM}^2
- dipole-dipole type image charge contributions proportional to Q^2
- dipole-charge contributions proportional to $V_{EFM} \times Q$.

Figure 4 (a) 3D atomic force microscopy picture of a silicon nanoparticle with 40 nm height; (b) schematics of the sample topography acquisition in tapping mode and (c) electrostatic force microscopy data acquisition during which the EFM cantilever is biased at V_{EFM} and moved over the substrate plane, and its frequency shifts are recorded

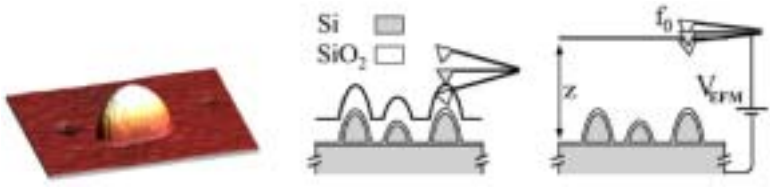

(a) (b) (c)

We show in Figure 5 that these contributions can be dissociated using EFM experiments on charged nanoparticles. EFM frequency shifts are displayed in Figure 5(a) as a function of V_{EFM} for a nanoparticle prior to charging, as well when positively and negatively charged. EFM data of the positively and negatively charged nanoparticle are shown in Figure 5(b) after subtraction of the EFM data of the uncharged nanoparticle, and show a linear behaviour corresponding to the charge contributions proportional to $V_{EFM} \times Q$ and Q^2. The image interaction is then measured (see inset) at the substrate surface potential, and shows a weak negative frequency shift, irrespective of the sign of the stored charge Q. To unambiguously identify this EFM frequency shift as stemming from dipole-dipole interactions, the spectroscopic analysis of Figure 5(a) and (b) has been

conducted on the same nanoparticle, but with a charge Q between –200e and +200e (effective surface dipole $Q \times h/\varepsilon$ between -400.10^2 and 400.10^2 Debye). Q has been tuned in practice by changing the injection bias V_{inj} in the $-6\ V < V_{inj} < 6\ V$ range. The EFM frequency shift at the surface potential is shown in Figure 5(c), and shows the attractive character (i.e., negative frequency shift) and a quadratic behaviour as a function of the stored charge Q, which demonstrates the dipole-dipole character of this contribution.

Figure 5 (a) Cantilever frequency shift $æf_{Ú} + æf_Q$ as a function of $V_{EFM} - V_S$ (V_S is the surface potential here $V_S = +0.55$ V) before (full line) and after charging at a bias $V_{inj} = -5$ V and +5 V (dotted and dashed lines respectively). Data were recorded within 40 s after charging. Lines are a guide to the eye. (b) Linear charge EFM signal $æf_Q$, obtained by subtracting the EFM signals $æf_{Ú} + æf_Q$ after and before the charging experiment. The solid line is a fit to the experimental data with slopes –2.7 Hz/V ($V_{inj} = -5$ V) and +3.7 Hz/V ($V_{inj} = +5$ V). This corresponds to an injected charge $Q = -140e$ ($V_{inj} = -5$ V) and $Q = 200e$($V_{inj} = +5$ V), i.e., a total nanoparticle charge $Q_0 + Q = -170e$ and $+170e$ respectively, taking into account the $Q_0 = -30e$ native charge contribution of the nanoparticle. Inset: zoom around the surface potential (vertical dotted line), evidencing the image force gradients: -1.5 ± 0.3 Hz for $Q_0 + Q = -170e$ and -0.95 ± 0.3 Hz for $Q_0 + Q = +170e$. (c) Points: Frequency shift associated with dipole-dipole interactions, plotted as a function of the surface dipole momentum $(Q + Q_0)/Å$associated with total stored charge $Q + Q_0$. Dashed line: numerical calculation of the dipole-dipole interaction frequency shift as a function of $Q + Q_0$

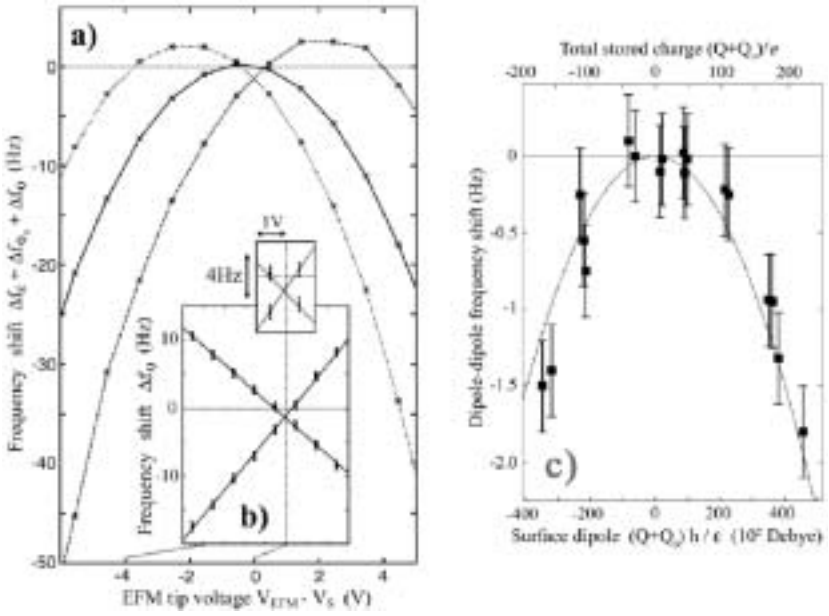

Other aspects of our research on 0D nanostructures have focused on developing an analytical modelling to measure accurately the amount of stored charges from EFM signals, and in arbitrary tip-nanoparticle geometries [19]. Also, to investigate the charging mechanisms in single silicon nanoparticles: dissociation between surface and volume charging from the hysteresis behaviour of the charging characteristics $Q(V_{inj})$ [20]; Schrödinger-Poisson calculations of the nanoparticle charge states in the

form of a 2D electron gas located at the nanoparticle-substrate interface during the charging experiment [21].

We now turn to the case of one-dimensional nanostructures such as carbon nanotubes (CNTs), in which delocalised charge patterns can be observed following a local charge injection (see Figure 6(b) and (c). Nanotubes deposited on 200 nm-thick SiO_2 layers can carry linear charge densities $\lambda \sim 10 - 10^2$ e/μm for $V_{inj} = 1$ V, and exhibit continuous or abrupt discharge mechanisms on nanotube structural defects [22]. Another key-feature is also the observation the emission of electrons from the CNTs to the SiO_2 layer, which appear as residual charges trapped on the oxide layer. This is visible from Figure 7(c), where the CNT is seen to be surrounded by a bright halo in the EFM image recorded after discharge. In this image, it is also clearly seen that the charge emitted by the CNT is enhanced at its two caps. This effect is attributed to a field-enhanced electron emission at the CNT caps, is analysed statistically in Figure 7(d) as a function of the CNT diameter. The cap enhancement is visible for CNT diameters below 25 nm, but vanishes for low-diameter (single-walled) nanotubes [22].

Figure 6 (a) Atomic force microscopy image of MWNT of 19 nm diameter on a 200 nm silicon dioxide surface; (b) EFM image ($V_{EFM} = -3$ V) acquired before charging (10 Hz colour scale) with a tip-substrate distance $z = 100$ nm; (c) EFM image taken in the same conditions, after a charge injection performed at the point indicated by an arrow in (a), using $V_{inj} = -5$ V for 2 min and (d) cross-sections of the EFM scans in (b) and (c). The position of the cross-section is shown by the horizontal bar in (b). The full width at half minimum of EFM signals before and after charging (resp. 100 nm and 440 nm) is marked by triangles as a guide to the eye

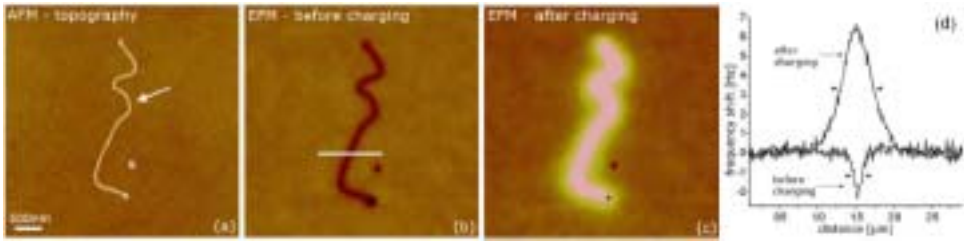

Figure 7 (a) Topography image of a 21 nm diameter MWNT; (b) EFM image (20 Hz frequency scale) before charge injection; (c) same image after charge injection ($V_{inj} = 5$ V during 2 min) and the MWCNT discharge. It shows an enhanced charge emission near both caps (+3 Hz frequency shift) in comparison with the charge emitted along the nanotube (+1.4 Hz frequency shift) and (d) ratio I_{cap}/I_{side} of the emitted charge intensities at the CNT cap compared to the CNT side, as a function of the CNT cap diameter. The inset shows a zoom of the data for SWCNTs with diameter <1.6 nm

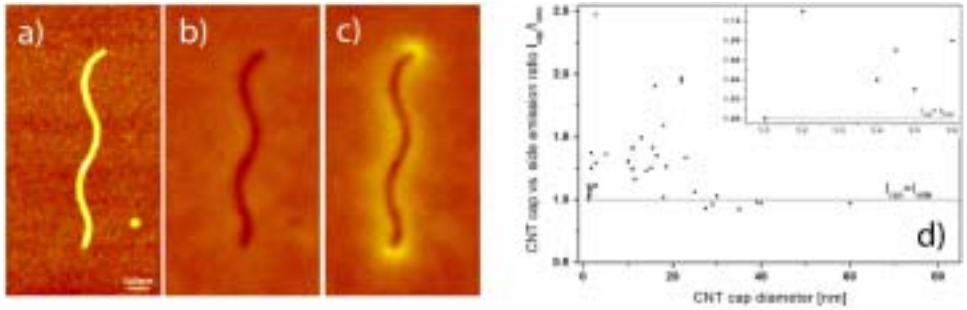

4 Scanning tunnelling spectroscopy of quantum dots

Different methods to growth or synthesise low dimensional semiconductors allow the fabrication of small objects where the dimensions can widely vary, leading thus to quantum size effects. As the sizes of the semiconductor structures are in the nanometer range, specific tools are required to observe these nano-objects and characterise simultaneously the quantum size effects. Scanning tunnelling microscopy offers the possibility to image the surfaces of individual nanostructures and, when used in the spectroscopic mode, can probe the electronic structure of single objects. While this technique has been extensively used to study metallic objects [23] or surfaces states of semiconductor surfaces [24], it has been proven more recently to be well suited to determine the electronic structure of semiconductor nano-objects, if their surface states are lying far from the band edges [25,26].

In this paper, we show the results of spectroscopic measurements obtained on two types of semiconductor nano-objects. Although variations of their size modify significantly their electronic structure, others effects must generally be taken into account to interpret the tunnelling spectra, such as the electron-electron Coulomb interaction. However, in this paper, the electron-electron Coulomb interaction is turned off, either by working with a small tunnelling barrier between the nano-objects and the substrate where they are lying onto, or by choosing a very low current set-point, what corresponds to a thick tunnelling barrier between the tip and the nano-object. Thus, the experiments are all conducted in a regime, called shell-tunnelling regime, where the electron levels of the nano-object are occupied by a single electron.

As a first example of semiconductor nano-objects, we consider InAs quantum dots (QDs) grown on a GaAs substrate in the Stransky-Krastanow growth mode. These QDs exhibit a three dimensional confinement with a δ-function-like electronic density of states. In recent years, scanning tunnelling spectroscopy (STS) has provided an unique mean to obtain not only the electronic spectra of low dimensional structures but also the localisation of the spectral features. The observation of the charge densities was for example achieved in artificial structures like the quantum corral [27] or even at room temperature on natural scattering centres like surface steps [28]. As a result, the probability density of electrons in InAs QDs can be investigated by STS.

The InAs quantum dots were grown by molecular beam epitaxy on a (001) oriented GaAs substrate, with a residual p-type concentration. The active part of the samples consists of 15 arrays of InAs boxes separated by 15 nm GaAs barriers. The whole structure is covered by a 140 nm GaAs overlayer. In order to build each dot array, an InAs coverage of 2.3 monolayers, slightly higher than the 1.7 monolayer required for the transition between a layer-by-layer growth mode and a layer-plus-island growth mode, were deposited on the GaAs layer within 20 s at a temperature of 520°C. They were immediately buried with GaAs. With these growth conditions, the density of dots is as high as 10^{10} cm^{-2} in the (001) plane. As cubic zinc-blende-structure compound semiconductors cleave easily along their nonpolar (110) planes, a large number of InAs QDs cross-sections are observed with the STM. When the cleavage is achieved in ultra high vacuum after thinning back the rear side of the sample, defect-free surfaces are usually obtained and since these surfaces are electronically unpinned, tunnelling spectroscopy allows the determination of the bulk

electronic properties, such as the band gap or the electron subbands of quantum wells [29]. To investigate the electronic structure of a dot, tunnelling current voltage curves were acquired simultaneously with the topographic image above individual quantum dots.

On Figure 8, the topography image clearly shows the lens shape of the QD. The differential conductivity images allow to visualise the density of states associated with the 1s electron ground state (peak at the energy E_1 in the dI/dV vs. V spectrum) as well as the first 2p electron excited state (peak at the energy E_2 in the dI/dV vs. V spectrum).

Figure 8 Tunnelling spectroscopic measurements acquired in the centre of a QD at a temperature of 77 K. Inset: Differential conductivity images obtained for the QD, shown in the topographic image (T), with its boundaries outlined by a white line. E_1 and E_2 correspond to the electron ground and first excited states. The feedback parameters were V_S = +1.5 V and I_{stab} = 100 pA

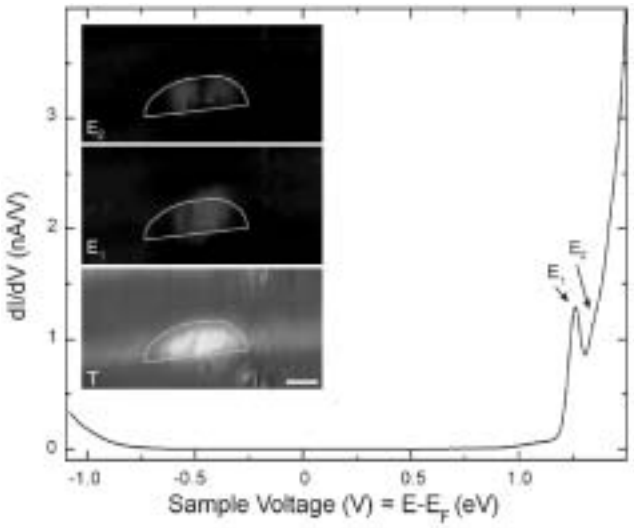

As a second example of tunnelling spectroscopic measurements on semiconductor nanostructures, we investigate cadmium selenide (CdSe) nanocrystals made by colloidal chemistry and deposited onto a gold surface by a simple drop casting method (in collaboration with D. Vanmaekelbergh, Debye Institute, University of Utrecht). The peaks measured in the conductance spectrum (Figure 9) at positive bias correspond to the injection of a single electron into the empty states of the CdSe nanocrystal conduction band. In the present case, three peaks are clearly observed above the threshold, corresponding to the 1s, 1p, and 1d states, respectively, as expected by the theory for these nano-objects often considered as artificial atoms [30]. The same type of results has been recently obtained on PbSe nanocrystals, shedding light on the quantum confinement effects in IV–VI semiconductor nanostructures [31].

Figure 9 Differential conductivity spectrum of a 6 nm-CdSe nanocrystal measured at a temperature of 5 K. Inset: STM topographic image of CdSe nanocrystals deposited on a gold surface. The scale bar is 10 nm

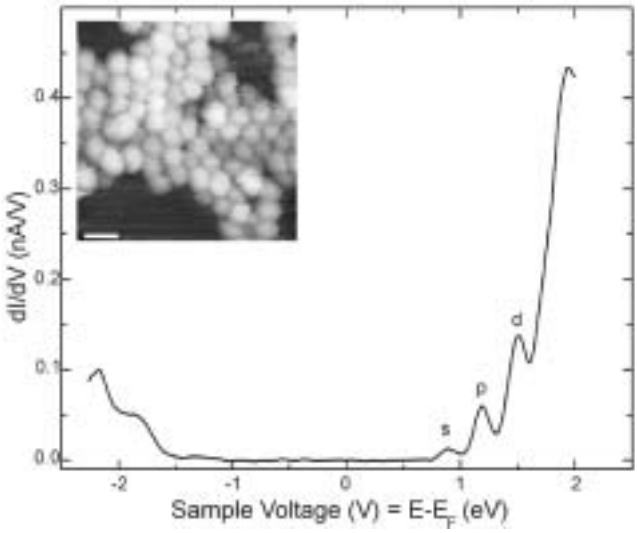

5 Surface science for bio-screening

One key step in the preparation of miniaturised high-throughput systems for bio-screening is the immobilisation of biological probes on a solid support for the sensitive and specific capture of soluble receptors. To increase the sensitivity of the detection methods, we elaborate new nanostructured supports based on functionalised patterns at the nanometer scale, semiconductor nanowires and nanogaps. On these supports, generally consisting of a Si substrate, we characterise the immobilisation of biological probes, which are linked by chemioselective methods developed at the Institut of Biology in Lille (IBL) [32]. Along with these characterisations, we understand the physical mechanisms ruling the behaviour of a liquid in nanostructured supports and find out solutions in the design of new nanostructures which enhance the optical signal emitted by the optical biological receptors adsorbed on the Si supports [33–36].

Here, we illustrate the electrical detection of immunoglobulin G (IgGs) from human serum using a nanogap-based biosensor. Human serum was chosen as a complex biological mixture because it contains 60–80 mg of protein/ml in addition to small molecules including salts, lipids and sugars. It is estimated that up to 10,000 proteins may be present in serum, IgG is one of the most abundant protein in human serum with normal levels between 8–17 mg/ml in adult blood. The detection method relies on the capture of IgG molecules by a probe immobilised between gold nanoelectrodes of 30–90 nm spacing [37,38]. The captured IgGs were further reacted with secondary antibodies (Ab^{II}) labelled with gold nanoparticles (Ab^{II} – GNPs, GNP = gold nanoparticle), protein A (pA) compared to goat anti-murine antibodies (goat-Ab).

Protein A (2.4×10^{-2} mM), goat anti-mouse antibodies (1.7×10^{-4} mM) and phosphate buffered-saline (PBS) were printed onto the nanoelectrodes using a piezo-driven non-contact printer (Packard Biochip Arrayer, volume 1 nl) after appropriate dilution in PBS. The diameter of the spots was typically 370 µm. Samples were then incubated during 6 h in a humid chamber (60% relative humidity).

Samples were washed successively with PBS containing 0.05% of Tween® 20 (by vol), water and ethanol. Substrates were then incubated for 1 h at 37°C in human serum diluted to 5% (by vol) with a PBS Tween® 20 0.05% BSA 2% buffer. Incubations were performed using a CMT^{TM} hybridisation chamber (Corning).

After washing again with PBS Tween® 20 0.05%, water and ethanol, samples were incubated for 1 h at 37°C with goat anti-human secondary antibodies labelled with 25 nm gold nanoparticles that were concentrated 10 fold (final concentration ~3.3×10^{12} GNP/ml) by centrifugation starting from the commercially available suspension. Samples were then washed successively with PBS Tween® 20 0.05%, water and ethanol and dried under N_2. SEM (Zeiss 820) analysis was carried out and combined with electrical measurements, performed in a low pressure vacuum chamber (0.2 mbar, H_2O and $O_2 < 0.1$ ppm) at room temperature with a picoamperemeter HP4140B. The applied voltage ranged from –5 V to +5 V with 500 mV steps. The principle of the detection is described in Figures 10 and 11 gives SEM image of the GNP layer around and between the nanoelectrodes after incubation of human serum and Ab^{II} – GNPs with pA (a) and goat-Ab (b) as probes.

On bare electrodes, the measured current with an applied voltage ranging from –5 V to +5 V is below 10^{-13} A and exhibits a random shape. After incubation with the serum and the Ab^{II}-GNPs, an increase in current ranging from 10^{-11} A to 10^{-7} A was generally observed with pA and goat-Ab. After incubation with the serum and the Ab^{II}-GNP, non-linear I(V) curve attributed to the presence of GNPs into the nanogaps, with a threshold voltage of the order of ±2 V, are observed.

Figure 10 Schematic illustration of the electrical detection of IgGs

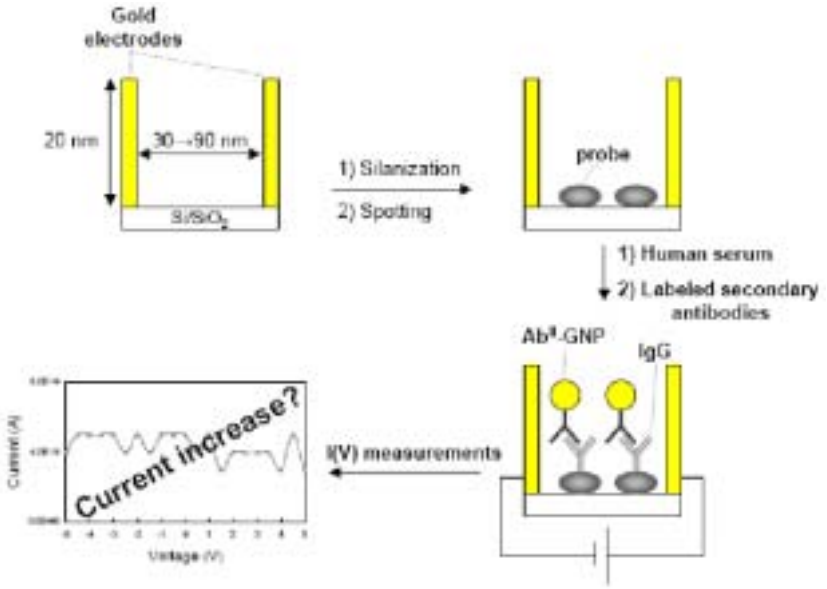

Figure 11 SEM image of the GNP layer around and between the nanoelectrodes after incubation of human serum and Ab^{II} – GNPs with pA (a) and goat-Ab (b) as probe

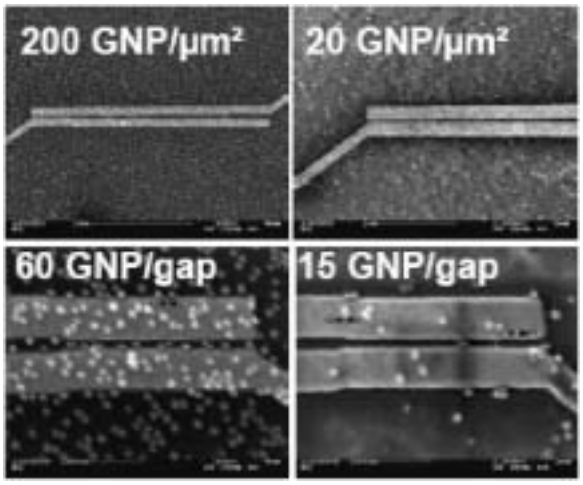

(a) (b)

We performed a non-linear regression analysis of the $I(V)$ data using a third order polynomial expression, characterised by the so-called multiple correlation coefficient r^2 (cut-off value $r_c^2 = 0.4776$ at a 1% significance level). We consider the proportion of nanogaps for which I and V are correlated after incubation with Ab^{II}-GNPs (see Figure 12, lower part). For pA and after incubation with serum and Ab^{II}-GNPs, 38 of 56 gaps (68%) were found to be correlated and exhibited intensities at $V = 5$ V ranging from 4.4×10^{-12} A to 1.7×10^{-7} A (current gain from ~17 to 1.3×10^6). For the non-correlated nanogaps (32%), current was lower than 2×10^{-13} A. For the goat-Ab, only 3 of 25 gaps (12%) were found to be correlated with an associated current of a few pA. Finally, no nanogaps were correlated for PBS. Secondly the current gain observed at 5 V for the correlated nanogaps (ratio between the current at 5 V after incubation with Ab^{II} – GNPs and the current measured for bare electrodes) is also given in Figure 12 (upper part). According to these observations, large changes in conductance were observed after incubation with Ab^{II}-GNPs with pA or goat-Ab as probes.

Finally, a quality factor combining both data and corresponding to the product of the percent of correlated nanogaps and the average current gain at $V = 5$ V was calculated and led to a quality factor of 5123 for pA, 11 for goat-Ab and 0 for PBS. The quality factor is greatly dependent upon the GNP density on the surface as determined by SEM analysis and reflects the specific capture of human antibodies from serum.

Using a complex biological fluid, we thus show that electrical detection based on the use of nanogaps and Ab^{II}-GNPs enable us to distinguish between different probes. Future studies will focus on demonstrating the reliability of the method. Ideally, the signal should scale with the concentration of IgGs in the sample. Consequently, the detection limit must be determined in order to assess the future use of our system.

Figure 12 Intensity of the detected current at $V = 5$ V after spotting with the human serum and incubation with the Ab^{II}-GNPs with pA, PBS and goat-Ab as probes (upper part). Associated correlation coefficient r^2 (lower part)

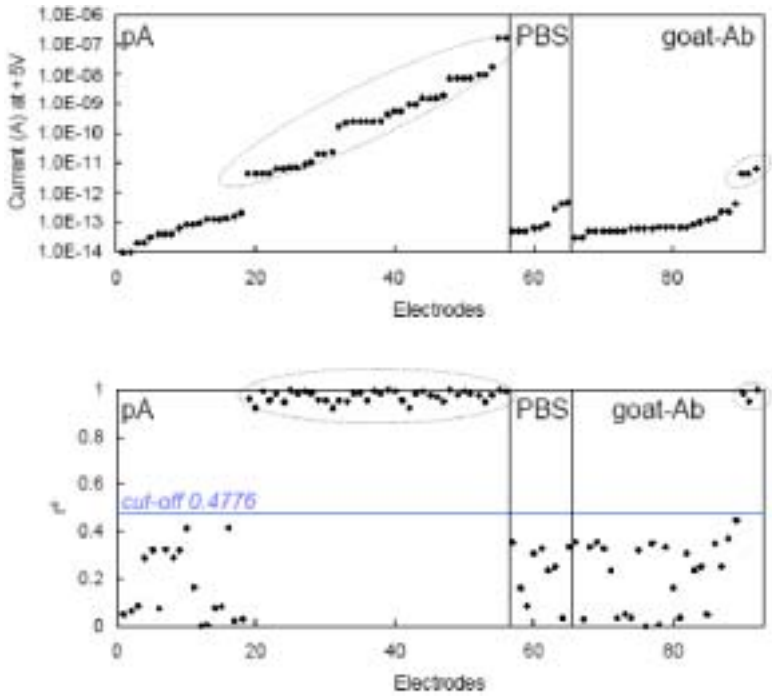

References

1 Yang, P. (2005) 'Chemistry and physics of semiconductor nanowires', *Mater. Res. Soc. Bull.*, Vol. 30, pp.85.

2 Yang, C., Zhong, Z. and Lieber, C.M. (2005) 'Encoding electronic properties by synthesis of axial modulation doped silicon nanowires', *Science*, Vol. 310, pp.1304–1307.

3 Cui, Y., Duan, X., Hu, J. and Lieber, C.M. (2000) 'Doping and electrical transport in silicon nanowires', *J. Phys. Chem. B*, Vol. 104, pp.5213–5216.

4 Martins, A.S., Menchero, J.G., Capaz, R.B. and Koiller, B. (2002) 'Atomistic description of shallow levels in semiconductors', *Phys. Rev. B*, Vol. 65, pp.245205.

5 Niquet, Y.M., Lherbier, A., Quang, N.H., Fernàndez-Serra, M.V., Blase, X. and Delerue, C. (2006) 'Electronic structure of semiconductor nanowires', *Phys. Rev. B*, Vol. 73, pp.165319.

6 Diarra, M., Niquet, Y.M., Delerue, C. and Allan, G. (2007) 'Ionization energy of donor and acceptor impurities in semiconductor nanowires: importance of dielectric confinement', *Phys. Rev. B*, Vol. 75, pp.045301.

7 Rubio, A., Corkill, J.L. and Cohen, M.L. (1994) 'Theory of graphitic boron nitride nanotubes', *Phys. Rev. B*, Vol. 49, pp.5081.

8 Chopra, N.G., Luyken, R.J., Cherry, K., Crespi, V. H., Cohen, M.L., Louie, S.G. and Zettl, A. (1995) 'Boron nitride nanotubes', *Science*, Vol. 269, pp.966.

9 Lee, R.S., Gavillet, J., Lamy de la Chapelle, M., Loiseau, A., Cochon, J-L., Pigache, D., Thibault, J. and Willaime, F. (2001) 'Catalyst-free synthesis of boron nitride single-wall nanotubes with a preferred zig-zag configuration', *Phys. Rev. B*, Vol. 64, Article 121405(R), pp.121405.

10 Wirtz, L., Lazzeri, M., Mauri, F. and Rubio, A. (2005) 'Raman spectra of BN nanotubes: Ab initio and bond-polarizability model calculations', *Phys. Rev. B*, Vol. 71, Article 241402(R), pp.241402.

11 Arenal, R., Ferrari, A.C., Reich, S., Wirtz, L., Mevellec, J-Y., Lefrant, S., Rubio, A. and Loiseau, A. (2006) 'Raman spectroscopy of single-wall boron nitride nanotubes', *Nano Lett.*, Vol. 6, pp.1812.

12 Lauret, J.S., Arenal, R., Ducastelle, F., Loiseau, A., Cau, M., Attal-Tretout, B., Rosencher, E. and Goux-Capes, L. (2005) 'Optical transitions in single-wall boron nitride nanotubes', *Phys. Rev. Lett.*, Vol. 94, Article 037405, pp.037405.

13 See, e.g., Onida, G., Reining, L. and Rubio, A. (2002) 'Electronic excitations: density-functional vs. many-body Green's-function approaches', *Rev. Mod. Phys.*, Vol. 74, pp.601.

14 Delerue, C., Allan, G. and Lannoo, M. (2003) 'Dimensionality-dependent self-energy corrections and exchange-correlation potential in semiconductor nanostructures', *Phys. Rev. Lett.*, Vol. 90, Article 076803, pp.076803.

15 Wirtz, L., Marini, A. and Rubio, A. (2006) 'Excitons in boron nitride nanotubes: dimensionality effects', *Phys. Rev. Lett.*, Vol. 96, Article 126104, pp.126104.

16 Arenal, R., Stéphan, O., Kociak, M., Taverna, D., Loiseau, A. and Colliex, C. (2005) 'Electron energy loss spectroscopy measurement of the optical gaps on individual boron nitride single-walled and multiwalled nanotubes', *Phys. Rev. Lett.*, Vol. 95, Article 127601, pp.127601.

17 Mélin, T., Deresmes, D. and Stiévenard, D. (2002) 'Charge injection in individual silicon nanoparticles deposited on conductive substrates', *Appl. Phys. Lett.*, Vol. 78, pp.5054.

18 Mélin, T., Diesinger, H., Deresmes, D. and Stiévenard, D. (2004) 'Probing nanoscale dipole-dipole interactions by electric force microscopy', *Phys. Rev. Lett.*, Vol. 92, pp.166101.

19 Mélin, T., Diesinger, H., Deresmes, D. and Stiévenard, D. (2004) 'Electric force microscopy of individually charged semiconductor nanoparticles on conductive substrates: an analytical model for quantitative charge imaging', *Phys. Rev. B*, Vol. 69, pp.035321.

20 Diesinger, H., Mélin, T., Deresmes, D., Stiévenard, D. and Baron, T. (2004) 'Hysteretic behavior of the charge injection in single silicon nanoparticles', *Appl. Phys. Lett.*, Vol. 85, pp.3546.

21 Barbet, S., Mélin, T., Diesinger, H., Deresmes, D. and Stiévenard, D. (2006) 'Charge-injection mechanisms in semiconductor nanoparticles analyzed from force microscopy experiments', *Phys. Rev. B*, Vol. 73, pp.045318.

22 Zdrojek, M., Mélin, T., Boyaval, C., Jouault, B., Wozniak, M., Gebicki, W., Huczko, A., Stiévenard, D. and Adamowicz, L. (2005) 'Charging and emission effects of multiwalled carbon nanotubes probed by electric force microscopy', *Appl. Phys. Lett.*, Vol. 86, pp.213114; Zdrojek, M., Mélin, T., Diesinger, H., Stiévenard, D., Gebicki, W. and Adamowicz, L. (2006) 'Charging and discharging processes of carbon nanotubes probed by electrostatic force microscopy', *J. Appl. Phys.*, Vol. 100, pp.114326.

23 Li, J., Schneider, W-D., Berndt, R. and Crampin, S. (1998) 'Electron confinement to nanoscale Ag Islands on Ag(111): a quantitative study', *Phys. Rev. Lett.*, Vol. 80, pp.3332.

24 Becker, R.S., Golovchenko, J.A., Hamann, D.R. and Swartzenruber, B.S. (1985) 'Real-space observation of surface states on Si(111) 7 × 7 with the tunneling microscope', *Phys. Rev. Lett.*, Vol. 55, pp.2032–2034.

25 U. Banin, U., Cao, Y., Katz, D. and Millo, O. (1999) 'Identification of atomic-like electronic states in indium arsenide nanocrystal quantum dots', *Nature*, Vol. 400, pp.542–544.

26 Hens, Z., Vanmaekelbergh, D., Stoffels, E.J.A.J. and van Kempen, H. (2002) 'Effects of crystal shape on the energy levels of zero-dimensional PbS quantum dots', *Phys. Rev. Lett.*, Vol. 88, pp.236803.

27 Crommie, M.F., Lutz, C.P. and Eigler, D.M. (1993) 'Imaging standing waves in a two-dimensional electron gas', *Nature*, Vol. 363, pp.524.

28 Avouris, P. and Lyo, I.W. (1994) 'Observation of quantum-size effects at room temperature on metal surfaces with STM', *Science*, Vol. 264, pp.942–945; Hofmann, Ph., Briner, B.G., Doering, M., Rust, H-P., Plummer, E.W. and Bradshaw, A.M. (1997) 'Anisotropic two-dimensional friedel oscillations', *Phys. Rev. Lett.*, Vol. 79, pp.265.

29 Feenstra, R.M., Collins, D.A., Ting, D.Z.Y., Wang, M.W. and McGill, T.C (1994) 'Interface roughness and asymmetry in InAs/GaSb superlattices studied by scanning tunneling microscopy', *Phys. Rev. Lett.*, Vol. 72, pp.2749.

30 Delerue, C. and Lannoo, M. (2004) *Nanostructures: Theory and Modelling*, Springer, Berlin.

31 Liljeroth, P., Overgaag, K., Urbieta, A., Grandidier, B., Hickey, S.G. and Vanmaekelbergh, D. (2006) 'Variable orbital coupling in a two-dimensional quantum-dot solid probed on a local scale', *Phys. Rev. Lett.*, Vol. 97, pp.096803.

32 Huot, D., Ollivier, L., El-Madhi, N., Gouyette, O., Huynh-Dinh, C., Gras-Masse, T., Lemoine, H., Melnyk, Y., Olivier, O. and Hot, C. (2003) 'Ŭ-oxo semicarbazone peptide or oligodeoxynucleotide microarrays', *Bioconjugate Chem.*, Vol. 14, pp.430–439.

33 Duburcq, X., Olivier, C., Desmet, R., Halesa, M., Carion, O., Grandidier, B., Heim, T., Stiévenard, D., Auriault, C. and Melnyk, O. (2004), 'Polypeptide semicarbazide glass microarrays: characterization and comparison with amine slides in serodetection studies', *Bioconjugate Chem.*, Vol. 15, pp.317.

34 Coffinier, Y., Olivier, C., Perzina, A., Grandidier, B., Wallart, X., Durand, J.O., Melnyk, O. and Stiévenard, D. (2005) 'Semicarbazide-functionnalized Si(111) surfaces for the site-specific immobilization of peptides', *Langmuir*, Vol. 21, No. 4, pp.1489.

35 Ardes-Guisot, N., Durand, J.O., Granier, M., Perzyna, A., Coffinier, Y., Grandidier, B., Wallart, X. and Stiévenard, D. (2005) 'Trichlorosilane isocyanate as coupling agent for mild conditions functionalization of silica-coated surfaces', *Langmuir (Lett.)*, Vol. 21, pp.9406–9408.

36 Perzyna, A., Olivier, C., Coffinier, Y., Grandidier, B., Granier, M., Melnyk, O., Stiévenard, D. and Durand, J-O. (2006), 'Detecting the chemoselective ligation of peptides to silicon with the use of Cobalt-based labels', *Langmuir*, Vol. 22, No. 16, pp.7059.

37 Haguet, V., Martin, D., Marcon, L., Heim, T., Stiévenard, D., Olivier, C., El-Mahdi, O. and Melnyk, O. (2004) 'Combined nanogap nanoparticles nanosensors for electrical detection of biomolecular interactions between polypeptides', *Appl. Phys. Lett.*, Vol. 84, pp.1213.

38 Brinkmann, M., Blossey, R., Marcon, L., Stiévenard, D., Dufrêne, Y.F. and Melnyk, O. (2006) 'Fluidics in a nanogap', *Langmuir*, Vol. 22, No. 23, pp.9784–9788.